Hindawi
Journal of Nanomaterials
Volume 2018, Article ID 5263132, 6 pages
https://doi.org/10.1155/2018/5263132

Research Article

Determination of Cyclability of Li/FeS_2 Batteries Based on Measurement of Coulombic Efficiency

Paul Maldonado Nogales, Hee-Youb Song, and Soon-Ki Jeong

Department of Chemical Engineering, Soonchunhyang University, Asan, Chungcheongnam 31536, Republic of Korea

Correspondence should be addressed to Soon-Ki Jeong; hamin611@sch.ac.kr

Received 8 May 2018; Revised 29 July 2018; Accepted 19 August 2018; Published 20 September 2018

Academic Editor: Manab Kundu

The electrochemical performance of negative electrodes based on different FeS_2 samples was investigated. The study demonstrated a correlation between the coulombic efficiency obtained over 60 cycles and the capacity loss rate evaluated over 15 cycles. The accuracy of the coulombic efficiency and capacity loss rate measurements was advantageous for predicting the aging behavior of half-cells over a short-term test. A suggested classification of the coulombic efficiency and verification via a numerical analysis were proposed to determine the fading rate of batteries during the galvanostatic test.

1. Introduction

Recently, lithium-ion batteries (LIBs) as a power source have been widely used in electrical devices, electric vehicles, energy storage systems, etc. In addition, there are a growing number of their applications that require excellent cyclability with high capacity. Hence, verifying the reliability of LIBs has become an important issue in recent years.

One of the most impressive studies on aging in LIBs tracks cells during cycling and storage for up to two years to quantitatively measure the lifetime of the battery based on electrode composition [1]. However, the evaluation of the cycle performance over a long time can be problematic if it takes days or months. Therefore, new techniques are needed for the effective aging evaluation of LIBs in a short period of time [2, 3].

The evaluation of the coulombic efficiency (CE) can be used to identify parameters that affect the normal functioning of the battery such as parasitic reactions between electrodes and electrolytes observed during discharge–charge cycling. Choi et al. [4] reported an FeS_2 cathode deficiency under different organic electrolytes. Their research includes calculations of the specific capacity and capacity loss rate. This kind of evaluation draws attention to special features that make it possible to determine the relation between accurate CE and capacity loss rate as a method of system optimization, and the results can be used to rank cells according to their life expectancy without the need to use tests that take long to perform [5].

This paper presents a method that utilizes the CE and capacity loss rate to determine the cyclability with a short-term test. Firstly, we investigated the CE based on the charge–discharge cycle in a normal operating process during 60 cycles. Then, to determine the aging during the discharge–charge cycle, the capacity loss rates were investigated with different particle sizes of the FeS_2 electrodes. A simple comparison of CE with the capacity loss rate can be used to determine the effectiveness of the method and to validate the results using a short-term test.

2. Materials and Methods

2.1. Preparation of FeS_2 Samples. FeS_2 (99.9%, VITZRO MILTECH) samples were mechanically milled using a planetary ball mill (PBM) (PULVERISETTE, Fritsch) for 3 hours (3 h PBM), 6 hours (6 h PBM), and 10 hours (10 h PBM) and milled using a single ball mill (SBM) for 72 hours (72 h SBM). The working electrodes were fabricated by mixing FeS_2 as an active material, carbon black as a conductive additive, and polyvinylidene fluoride (PVDF) as a binder in a 60 : 20 : 20 weight ratio, respectively. The prepared slurry

was cast on a copper foil with a doctor blade and dried at 120°C in a vacuum oven for 12 h.

2.2. Material Characterization. The particle size distributions (PSDs) were analyzed using a particle size analyzer (Nano-Plus-1, Particulate Systems). Structural analysis of FeS_2 was carried out by employing X-ray diffraction (XRD), using a diffractometer (D/max-2200/PC, Rigaku Co.) equipped with a Cu Kα source (40 kV, 40 mA), and the morphologies of the samples were studied using scanning electron microscopy (SEM) (SNE-3000M, SEC Co.).

2.3. Electrochemical Measurements. The electrochemical analysis was performed in a 2032-type coin cell. FeS_2 was used as a working electrode, and lithium foil was used as the reference electrode. The electrolyte solution was 1 mol dm^{-3} $LiClO_4$ dissolved in a 1 : 1 (v/v) mixture of ethylene carbonate and dimethyl carbonate (battery grade, Enchem Co.). Galvanostatic measurements were performed using a battery test system (WBCS3000, WonATech Co.) between 1 and 2.8 V at constant currents of 89.2 and 892 mA g^{-1}. All the potentials were referenced against Li/Li^+.

2.4. Measurement of Coulombic Efficiency (CE) and Capacity Loss Rate. For a Li/FeS_2 half-cell, the "discharge" corresponds to the lithiation of FeS_2. Based on the cycling data, the CE is measured as the ratio of the capacity of the charge Qc immediately following the previous discharge Qd [6]. The CE value is obtained using the formula CE = Qc/Qd, and changes over the number of cycles are evaluated. It is expected that CE < 1.0. The measurements obtained from all the tests performed on the samples were used to evaluate the capacity loss rate as the average of the percentage ratio of every discharge capacity and the previous capacity between the 10th and 60th cycle.

3. Results and Discussion

3.1. Physical and Structural Characterization. The XRD patterns and SEM images of the pristine, 72 h SBM, 3 h PBM, 6 h PBM, and 10 h PBM samples are shown in Figure 1. All the diffraction peaks are identical and coincide with the pattern of FeS_2 (PDF card no. 42-1340) in a simple cubic structure Pa3 space. Additionally, as shown in Figure 1, for the 3 h PBM, 6 h PBM, and 10 h PBM samples, the width of the peaks tended to be broader and shorter, a behavior that is not exhibited by the 72 h SBM. From another standpoint, FeS_2 particles are in shape of irregular fragments, not well identified by size. Thus, SEM images were not considered due to the fact that it cannot offer a quantitative description of particle size; instead, the inclusion of PSD analysis has more valuable information about particle dimension in Figure 2.

In order to obtain samples with different physical characteristics, five FeS_2 samples were selected to be subjected to a ball milling process before testing, because it was presumed that the reduction in particle sizes is beneficial for lithium-ion storage [7] and improves the performance of the Li/FeS_2 half-cell [8]. As shown in Table 1, the PSDs of milled FeS_2 (from Figure 2) were distributed in two regions clearly divided according to the size and percentage in the sample; for the pristine, 72 h SBM, 3 h PBM, 6 h PBM, and 10 h PBM samples, the results obtained in the region with the highest percentage (greater than 50%) are in the range of 30–100, 15.6–50.0, 0.1–1.1, 26.1–73.7, and 0.1–0.8 μm, respectively. Hence, the results indicate that as the ball milling time increases, the particle size decreases, but the smaller the particle size, the greater the agglomeration [7]. This behavior is exhibited by the 72 h SBM, 6 h PBM, and 10 h PBM samples with a distribution of 15.6–50.0, 26.1–73.7, and 7.0–25 μm, respectively: the particle size was higher than that of the 3 h PBM sample under the same process conditions.

3.2. Verification of FeS_2 Charge and Discharge Mechanism. First, we verified the reduction and oxidation inside the cell. The effect of Li^+ diffusivity on FeS_2 is shown in Figure 3. The $Li_2Fe_2S_2$ is formed in one voltage plateau during the initial discharge, and the reaction involves a reduction in metallic Fe and Li_2S at 1.4 V [9]. After discharge, a consecutive charge shows that FeS and Li_2S_n are formed, and these compounds are combined into a complex of polysulfides with partial oxidation to FeS_2 [9, 10] that represents a decrease in capacity from the 1st to the 2nd discharge and subsequent cycles [6, 11, 12] particularly because of the dissolution of intermediates such as lithium polysulfide (Li_2S_n, $4 < n < 8$) in the liquid electrolyte [11, 13–16].

3.3. Effect of Variation of Physical Characteristics on Coulombic Efficiency. A CE calculation was conducted to compare the effect of the particle size on the performance of FeS_2. The left side of Figure 4 shows a detailed voltage profile for the FeS_2 electrodes, while the right side shows the CE reached during the first four cycles.

Therefore, during the charge–discharge test, despite the shapes of the curves, the five samples show considerably identical results; the electrode created after 10 h PBM shows a discharge capacity of 540 mAh g^{-1}, and a nearly identical discharge was obtained for the 72 h SBM, 3 h PBM, 6 h PBM, and pristine samples. An inhomogeneous particle size combination shown by the PSD test in Table 1 might be the first cause of nondifferentiation of the end discharge capacity.

Although the left part of Figure 4 shows that the discharge and charge capacities are almost identical, a detailed comparison to tell the difference between them is hardly possible. Therefore, the graph of CE on the right side indicates some characteristics that differ for each sample. First, the results corresponding to the 0.7–1 range on the coulombic efficiency axis have an acceptable accuracy showing an evident contrast between each cycle. Second, the CE of the 10 h PBM sample increases as follows: 0.752, 0.960, 0.977, and 0.980 from the 1st to the 4th cycle, respectively; no doubt, the percentage of small particle size around 64.3% shown in Table 1 is ineffective if the CE in 10 h PBM is expected to increase as shown in Figure 4. Finally, among all the electrodes, 10 h PBM has the lowest CE in every cycle.

3.4. Numerical Analysis Evaluation over the Lifetime of the Cell. To understand the CE better, we extended the analysis

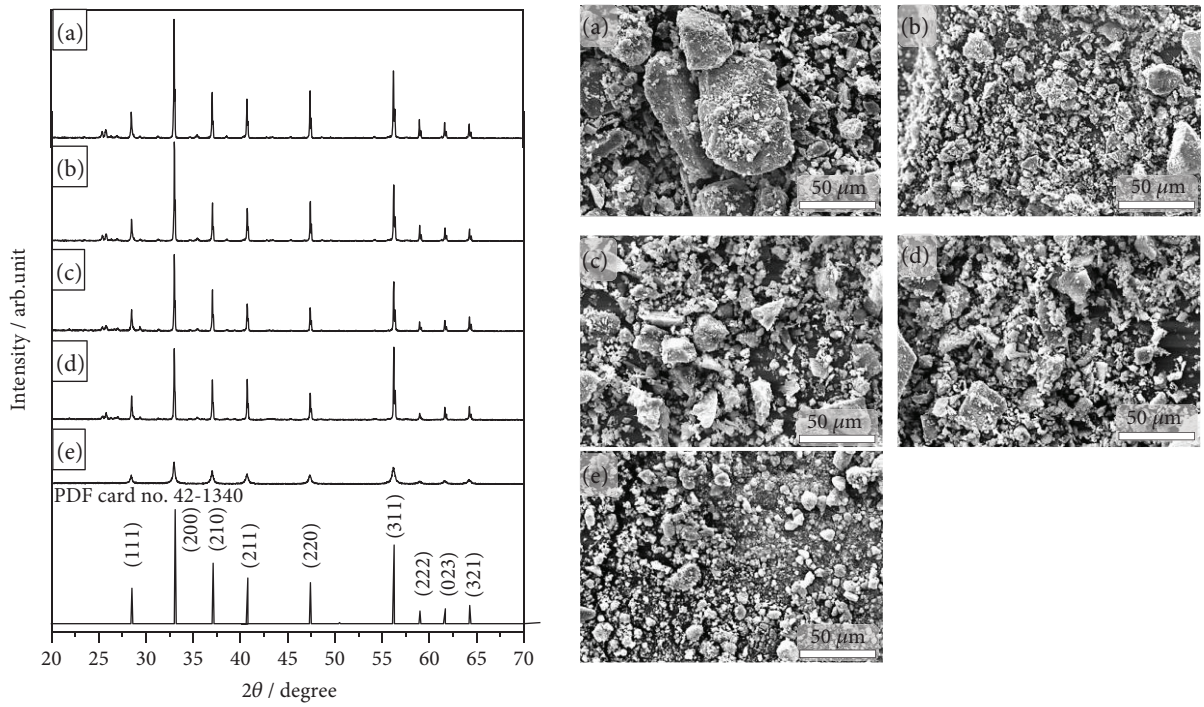

Figure 1: XRD patterns and SEM images of (a) pristine, (b) 72 h SBM, (c) 3 h PBM, (d) 6 h PBM, and (e) 10 h PBM.

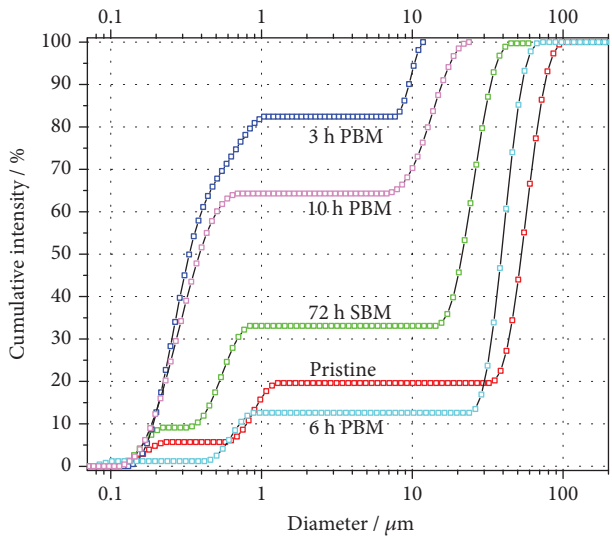

Figure 2: Accumulative intensity of particle size vs. diameter of particle in μm.

Table 1: Particle size distribution and percentage representation for different samples.

Sample	Particle size distribution (μm)	
Pristine	0.1–1.3 (20.0%)	30.0–100.0 (80.0%)
72 h SBM	0.1–0.8 (33.3%)	15.6–50.0 (66.7%)
3 h PBM	0.1–1.1 (81.0%)	8.2–11.8 (19.0%)
6 h PBM	0.6–0.9 (12.6%)	26.1–73.7 (87.4%)
10 h PBM	0.1–0.8 (64.3%)	7.0–25.0 (35.7%)

beyond the results shown in Figure 4 to study the relationship between the CE and discharge capacity against the cycle number, as shown in Figure 5. The continuous discharge–charge process is monitored from the 1st to the 15th cycle and from the 1st to the 60th cycle for short- and long-term tests, respectively. To evaluate comparable end points, the testing process follows a specific pattern during the data collection, as shown in the left side of the figure. The increase, decrease, and stabilization of the end discharge capacity points observed during the first 15 cycles can be attributed to the conditioning of the half-cells, a period that occurs after the electrolyte penetrates the electrode [17]. This increases the contact area between the electrode, electrolyte, and Cu foil, which yields an increment in the capacity. The right side of Figure 5 shows that the CE values for the 3 h PBM and pristine samples are the highest (over 0.99), followed by those of the 72 h SBM and 6 h PBM samples, whereas the CE of the 10 h PBM sample is the lowest.

After a visual comparison of the graph, numerical analysis was used to rank the electrodes and a nonlinear curve fitting analysis was used to verify the arrangement. This curve, which is obtained from the Chapman model $y = a * (1 - \exp(-b * x))\text{^}c$, shows the best fit to the shapes of the curves, as all the CE curve shapes are quite similar with a pronounced increase at the beginning and an asymptotic pattern around the value of 1. This adjustment makes it possible to give every electrode an adjusted R-square value over 0.99, a value that explains how close the data are to the fitted regression curve. This method was chosen because it is one of the most practical ways to approximate the model using a curve and refine the parameters via successive iterations. This analysis enables us to rank the aging.

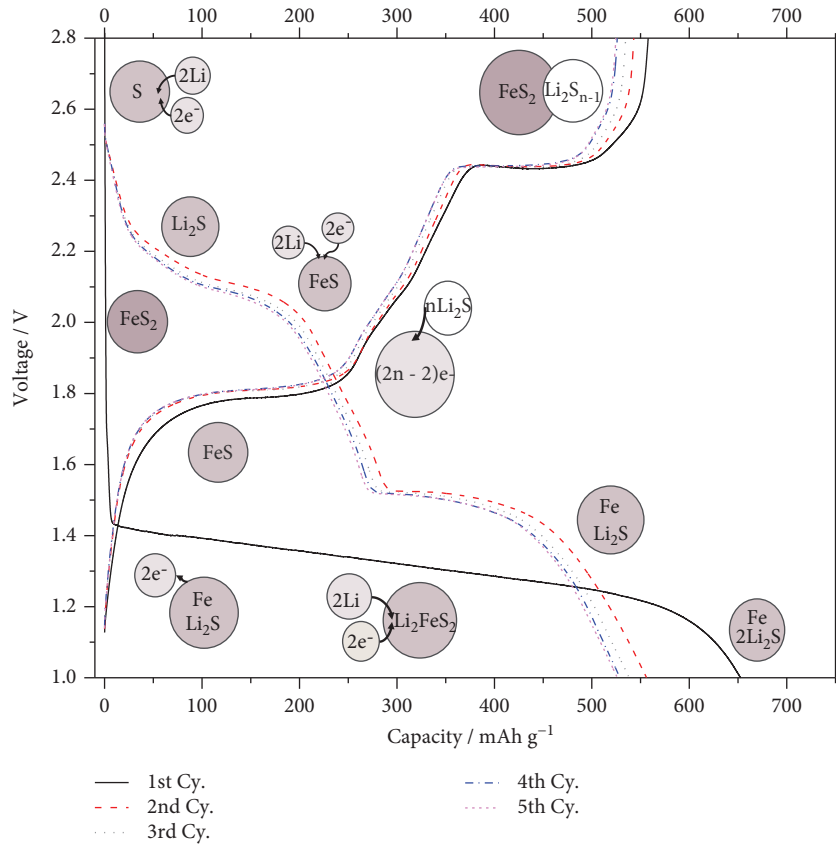

Figure 3: Charge and discharge mechanism of the FeS_2 electrode in 1 M $LiClO_4$/EC : DMC (1 : 1 *v*/*v*) at a constant current of 89.2 mA g^{-1} (0.1 C).

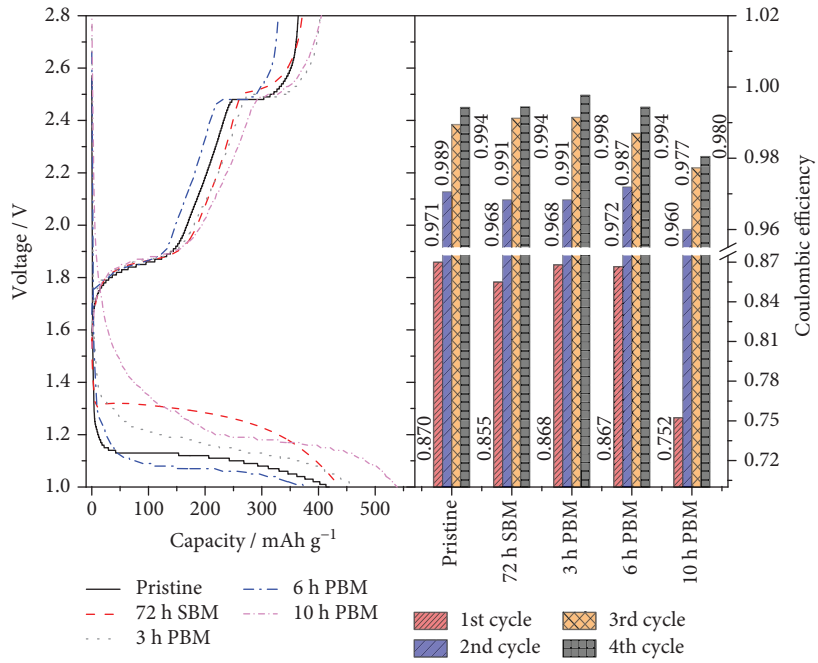

Figure 4: (Left) charge and discharge curves of the FeS_2 electrode in 1 M $LiClO_4$/EC : DMC (1 : 1 *v*/*v*) at a constant current of 892 mA g^{-1} (1 C). (Right) coulombic efficiency reached during the first four cycles.

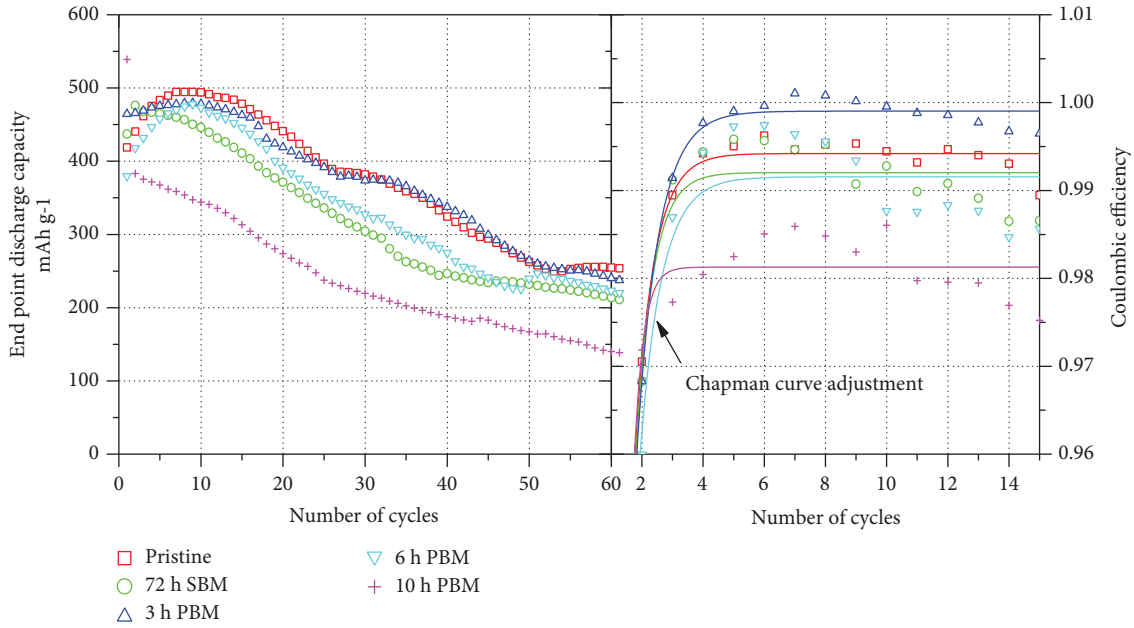

Figure 5: (Left) results of the coulombic efficiency vs. cycle number and (right) end point discharge capacity vs. cycle number for FeS_2 electrodes in 1 M $LiClO_4$/EC : DMC (1 : 1 *v*/*v*) at a constant current of 892 mA g^{-1}.

Table 2: Capacity loss rate per cycle of milled FeS_2 samples calculated over the last 60 cycles and nonlinear curve fitting report.

Sample	Value	Chapman *R*-square	Capacity loss rate per cycle (%)
3 h PBM	$a = 0.99904$ $b = 1.39988$ $c = 0.49678$	0.99830	0.97
Pristine	$a = 0.99421$ $b = 1.62866$ $c = 0.61185$	0.99727	1.62
72 h SBM	$a = 0.99204$ $b = 1.79919$ $c = 0.82355$	0.99063	1.80
6 h PBM	$a = 0.99155$ $b = 1.40964$ $c = 0.48300$	0.97778	1.83
10 h PBM	$a = 0.98128$ $b = 3.26758$ $c = 6.84182$	0.99634	2.03

Table 2 shows the Chapman model curve fitting results for a short-term test. The independent variables are denoted as "*a*," "*b*," and "*c*," where the variable "*a*" represents the horizontal asymptote of 1, a value that helps us rank all the samples from the 1st to the 5th as follows: 3 h PBM, pristine, 72 h SBM, 6 h PBM, and 10 h PBM based on values of 0.99904, 0.99421, 0.99204, 0.99155, and 0.98128, respectively.

In the long-term test, the end discharge capacity behavior indicated a fading rate of the capacity, which is expressed as the "capacity loss rate per cycle" at the FeS_2 electrode. This capacity loss rate is also shown in Table 2. A capacity loss rate, calculated over 60 cycles, of 0.97% per cycle, is recorded for the 3 h PBM sample, which is slightly lower than the value of 1.62% obtained for the pristine electrode. This indicates a better lithiation–delithiation for the 3 h PBM electrodes. In contrast, the half-cell that contains the 10 h PBM sample has a value of 2.03%, which is the highest discharge capacity loss registered from the beginning, indicating poor lithiation in the electrode. This may be due to the difference in capacity for the first two discharge capacities, i.e., 539 and 383 mAh g^{-1}, respectively. This behavior is expected, as explained above, where new reactions result in new compounds.

The short-term test can be used to identify and demonstrate the change in the CE in Li-ion cells during cycling, as shown in Figure 5. Hence, this test, rather than the long-term test until the end of the cell lifetime, should be able to predict a set of failures in the half-cell. There is enough evidence to confirm that this type of evaluation can be of significant use in differentiating and finding parameters that reduce the cell lifetime.

4. Conclusions

We created a ranking of the deterioration between electrodes based on their CE. This method can be used for quantifying the decay of the electrodes during the cycling process using a short-term test. A careful measurement of the CE would allow the evaluation of a cell over 15 cycles via a short-term test, which is less time-consuming than long tests (over 60 cycles). We confirm that a physical particle reduction

produces a slight increase in the CE in the 3 h PBM FeS_2 sample, which has the highest CE among all the samples.

Although the performance obtained was not optimal, the connection between the CE and capacity loss rate was determined, which facilitates an in-depth understanding of FeS_2 electrodes, indicating the effectiveness of this method.

Although this test enables us to determine the effects of the polysulfides on CE, this procedure does not quantify the polysulfides in the sample. Further investigations on CE and the use of X-ray photoelectron spectroscopy would help us find a connection between the battery decay and elements that affect the Li/FeS_2 half-cell.

Data Availability

The data that support the findings of this study are available from the corresponding author, Soon-Ki Jeong, upon reasonable request.

Conflicts of Interest

The authors declare that there is no conflict of interest regarding the publication of this paper.

Acknowledgments

This work was supported by the Korea Institute of Energy Technology Evaluation and Planning (KETEP) and the Ministry of Trade, Industry & Energy, Republic of Korea (no. 20184030202130). This work was supported by Soonchunhyang University Research Fund.

References

[1] S. Erik, B. Jason, C. Schmidt, and W. Howard, "A practical longevity model for lithium-ion batteries: de-coupling the time and cycle-dependence of capacity fade," *Journal of the Electrochemical Society*, vol. 140, p. 208, 2005.

[2] J. Jiang, Z. Lin, Q. Ju, Z. Ma, C. Zheng, and Z. Wang, "Electrochemical impedance spectra for lithium-ion battery ageing considering the rate of discharge ability," *Energy Procedia*, vol. 105, pp. 844–849, 2017.

[3] P. Keil and A. Jossen, "Calendar aging of NCA lithium-ion batteries investigated by differential voltage analysis and coulomb tracking," *Journal of the Electrochemical Society*, vol. 164, no. 1, pp. A6066–A6074, 2017.

[4] J. W. Choi, G. Cheruvally, H. J. Ahn, K. W. Kim, and J. H. Ahn, "Electrochemical characteristics of room temperature Li/FeS_2 batteries with natural pyrite cathode," *Journal of Power Sources*, vol. 163, no. 1, pp. 158–165, 2006.

[5] A. J. Smith, J. C. Burns, S. Trussler, and J. R. Dahn, "Precision measurements of the coulombic efficiency of lithium-ion batteries and of electrode materials for lithium-ion batteries," *Journal of the Electrochemical Society*, vol. 157, no. 2, p. A196, 2010.

[6] S. S. Zhang and D. T. Tran, "Electrochemical verification of the redox mechanism of FeS_2 in a rechargeable lithium battery," *Electrochimica Acta*, vol. 176, pp. 784–789, 2015.

[7] D. Zhang, J. P. Tu, J. Y. Xiang et al., "Influence of particle size on electrochemical performances of pyrite FeS_2 for Li-ion batteries," *Electrochimica Acta*, vol. 56, no. 27, pp. 9980–9985, 2011.

[8] Y. Shao-Horn, S. Osmialowski, and Q. C. Horn, "Nano-FeS_2 for commercial Li / FeS_2 primary batteries," *Journal of the Electrochemical Society*, vol. 149, no. 11, article A1499, 2002.

[9] T. Evans, D. M. Piper, S. C. Kim et al., "Ionic liquid enabled FeS_2 for high-energy-density lithium-ion batteries," *Advanced Materials*, vol. 26, no. 43, pp. 7386–7392, 2014.

[10] Q. Wang and Y. Wang, "Overcoming the limiting step of Fe_2O_3 reduction via in situ sulfide modification," *ACS Applied Materials and Interfaces*, vol. 8, no. 16, pp. 10334–10342, 2016.

[11] S. S. Zhang, "The redox mechanism of FeS_2 in non-aqueous electrolytes for lithium and sodium batteries," *Journal of Materials Chemistry A*, vol. 3, no. 15, pp. 7689–7694, 2015.

[12] X. B. Cheng, J. Q. Huang, H. J. Peng et al., "Polysulfide shuttle control: towards a lithium-sulfur battery with superior capacity performance up to 1000 cycles by matching the sulfur/electrolyte loading," *Journal of Power Sources*, vol. 253, pp. 263–268, 2014.

[13] T. Mori, Y. Orikasa, K. Nakanishi et al., "Discharge/charge reaction mechanisms of FeS_2 cathode material for aluminum rechargeable batteries at 55°C," *Journal of Power Sources*, vol. 313, pp. 9–14, 2016.

[14] J. Yang, M. Liu, Z. Wei et al., "Controlling electrochemical lithiation/delithiation reaction paths for long-cycle life nanochain-structured FeS_2 electrodes," *Electrochimica Acta*, vol. 211, pp. 671–678, 2016.

[15] F. Zhang, C. Wang, G. Huang, D. Yin, and L. Wang, "FeS_2@C nanowires derived from organic-inorganic hybrid nanowires for high-rate and long-life lithium-ion batteries," *Journal of Power Sources*, vol. 328, pp. 56–64, 2016.

[16] V. Pele, F. Flamary, L. Bourgeois, B. Pecquenard, and F. Le Cras, "Perfect reversibility of the lithium insertion in FeS_2: the combined effects of all-solid-state and thin film cell configurations," *Electrochemistry Communications*, vol. 51, pp. 81–84, 2015.

[17] K. Sun, Q. Zhang, D. C. Bock et al., "Interaction of TiS_2 and sulfur in Li-S battery system," *Journal of the Electrochemical Society*, vol. 164, no. 6, pp. A1291–A1297, 2017.